AUT Journal of Electrical Engineering

AUT J. Electr. Eng., 56(2) (2024) 153-164
DOI: 10.22060/eej.2023.22533.5548

A Low-Profile Metasurface MIMO Antenna with Suppressed Higher-Order Modes for 5G Applications

Hamed Hamlbar-Gerami, Robab Kazemi*

Faculty of Electrical and Computer Engineering, University of Tabriz, Tabriz, Iran

ABSTRACT: In this paper, a novel low-profile and low cross-polarization metasurface antenna is proposed for 5G mm-wave applications. The proposed antenna consists of two layers, with a slot antenna as the base and a novel metasurface layer on top. The metasurface layer is a 3×3 array of patches. By strategically incorporating slits and stubs within the middle patches, the undesired degenerate mode is separated from the fundamental mode, and higher-order modes are suppressed that typically appear in conventional metasurfaces. Additionally, rectangular slots are added in the middle of the corner patches to shift higher-order modes to frequencies beyond the desired operating bandwidth, mitigating issues such as beam splitting and beam squint in the radiation patterns. Experimental measurements demonstrate that the proposed metasurface antenna operates over a bandwidth of 25.14% (23.3 GHz to 30 GHz), with a return loss better than 10 dB, a peak gain of 8.1 dB, and an XP level lower than -26 dB and -53 dB at and planes, respectively. Compared to conventional metasurface antennas, our design reduces the antenna dimension by 62%, resulting in a compact size of 0.72λ0 × 0.72λ0 × 0.08λ0. Furthermore, we validate the performance of the single-element antenna by employing it in a 2×2 Multiple Input-Multiple Output (MIMO) configuration without requiring additional inter-element spacing. The MIMO antenna exhibits promising performance as well. Overall, our proposed low-profile and low cross-polarization metasurface antenna shows great potential for 5G mm-wave applications, offering improved efficiency and reduced size compared to conventional designs.

Review History:

Received: Jul. 05, 2023
Revised: Aug. 28, 2023
Accepted: Oct. 29, 2023
Available Online: Mar. 01, 2024

Keywords:

Characteristic Mode Analysis (CMA)
Metasurface Antenna
MIMO Antenna
Suppressed Cross-Polarization
5G mm-wave

1- Introduction

Nowadays, communication networks are undergoing a substantial expansion, with a growing need for high-speed data transfer rates to efficiently handle tasks such as online streaming and large file transfers. As a result, there is an increasing demand for systems that can provide high data transfer capacity. One effective method to enhance channel capacity is the use of the Multiple Input-Multiple Output (MIMO) technique, which involves employing multiple antennas [1, 2].

Metasurface antennas have demonstrated their effectiveness in improving the bandwidth and gain of conventional microstrip antennas [3, 4]. Several design methods have been utilized, including modal dispersion curve [5], surface impedance extraction [6], and characteristic mode analysis (CMA) [7-9]. However, the first two methods are unable to accurately predict the radiation performance of metasurfaces due to their reliance on infinite periodic boundary conditions. Additionally, selecting the appropriate excitation mode is a challenge for the modal dispersion curve method [3]. On the other hand, the CMA method, which is based on the Method of Moments (MOM) technique, has successfully been applied to various designs and allows for the prediction of modal behavior and radiation performance of metasurfaces [7]. This simplifies the process of mode analysis.

In the context of 5G systems and modern miniaturized communication systems, MIMO antennas have become essential to accommodate the increasing number of user terminals. This often requires placing the antennas in close proximity to each other [10]. In such cases, the excitation of higher-order modes in metasurface antennas has a significant impact on the antenna's radiation characteristics, including gain, XP level, beam splitting, and beam tilting [3]. To ensure stable radiation patterns of elements in a MIMO system, it is crucial to effectively shift undesired higher-order modes outside the operating bandwidth while preserving the desired fundamental mode.

In this paper, a novel low-profile non-uniform metasurface antenna operating within the 5G mm-wave frequency range (23.3 GHz - 30 GHz) is introduced. The performance of the metasurface is evaluated using the CMA method and compared to a conventional uniform metasurface structure. The conventional uniform metasurface suffers from

*Corresponding author's email: r.kazemi@tabrizu.ac.ir

degeneracy between the first and second radiation modes, along with the presence of higher-order modes within the desired frequency range. To address these issues, the proposed metasurface incorporates rectangular slits and stubs on the sides of the middle patches. Furthermore, narrow rectangular slots are added in the middle of corner patches. Finally, the performance of the proposed antenna is evaluated in a 2×2 MIMO configuration.

The paper is structured as follows: Section 2 analyzes the modal significance (MS), modal currents, and the far-field directivity patterns of the first five modes of both uniform and proposed metasurfaces using the CMA method. Section 3 discusses the structure and performance of the proposed metasurface antenna. Section 4 presents a comprehensive evaluation of the proposed metasurface antenna's performance in a 2×2 MIMO configuration. Finally, Section 5 concludes the paper.

2- Characteristic mode analysis and metasurface

In the CMA method, the eigenvalue equation is formulated as follows [11]:

$$[X]J_n = \lambda_n [R]J_n \tag{1}$$

where $[R]$ and $[X]$ represent the real and imaginary parts of the impedance matrix in the MOM method, respectively. λ_n is the eigenvalue and J_n is the eigencurrent of the nth mode. At the resonance frequency, the eigenvalue must be zero. Based on the CMA method, the total current on a perfect electric conductor (PEC) can be expressed as a linear combination of the currents associated with each mode [11]:

$$J = \sum_n \alpha_n J_n \tag{2}$$

where α_n is the modal weighting coefficient for each mode, representing the contribution of that specific mode to the overall radiated power. This parameter can be mathematically defined according to Eq. (3) [11].

$$\alpha_n = \frac{V_n^i}{1 + j\lambda_n} \tag{3}$$

where V_n^i is the modal excitation coefficient and can be obtained from Eq. (4) [11].

$$V_n^i = \left\langle J_n, E^i \right\rangle = \oiint_s J_n \cdot E^i ds \tag{4}$$

V_n^i is the inner product of the surface current of the nth mode and the impressed electric field E^i. To achieve adequate excitation for each mode, it is necessary to apply the impressed E-field in areas where the surface current is relatively strong. However, this approach may also excite unwanted modes leading to negative effects on the antenna performance.

The Modal Significance (MS) of each mode is calculated as follows [11]:

$$\mathrm{MS}_n = \frac{1}{\left|1 + j\lambda_n\right|} \tag{5}$$

The MS is not dependent on excitation and its value indicates the potential for mode excitation. A value of 1 for the MS indicates the highest efficiency of that mode.

Fig. 1 presents the structures of the uniform and proposed metasurfaces. The uniform metasurface in Fig. 1(b) is a 3×3 array of square patches, where the corner patches are designated as "C" and the remaining patches are referred to as middle patches. In contrast, the proposed metasurface, depicted in Fig. 1(c), incorporates modifications to both the middle and corner patches. They are printed on a RT/duroid 5880 substrate with a thickness of 0.787 mm, $\varepsilon_r = 2.2$, and $\tan\delta = 0.0009$. By utilizing the CMA tool in CST Studio Suite, we obtained the MS curves of the first five characteristic modes of the uniform structure, as shown in Fig. 2. As discussed in [11], a mode can be excited if its MS value at a given frequency is equal to or exceeds 0.707. In Fig. 2, it can be observed that the first and second modes are degenerate, and three higher-order modes appear within the desired frequency range of 25.5 GHz - 30 GHz. The undesired modes are excited together with the first mode, resulting in an increase in XP level, a decrease in antenna gain and efficiency, and perturbation in the radiation patterns of antennas in MIMO configurations. Therefore, it is crucial to move these modes outside the operating frequency band.

In Fig. 3(a), the modal currents of the uniform metasurface are shown at the frequency of 27 GHz. The surface currents of the first and second modes are concentrated in the middle, while the currents of the higher-order modes are located on the corner patches. As a result, the first two modes exhibit radiation in the broadside direction, while modes 3 to 5 have a null in the broadside direction, as shown in Fig. 3(b).

To address the degeneracy between the first and second modes, certain modifications were implemented on the middle patches. Narrow slits were introduced on the left and right sides of these patches, and small stubs were added to the top and bottom sides to suppress higher-order modes. Additionally, a narrow slot was incorporated in the middle of corner patches to further minimize the effects of unwanted modes. The new metasurface configuration is depicted in Fig. 1(c). The optimized dimensions of the uniform and proposed metasurfaces are summarized in Table 1.

The lateral dimensions of the uniform metasurface are $1.17\lambda_0 \times 1.17\lambda_0$, while the proposed structure has smaller dimensions of $0.72\lambda_0 \times 0.72\lambda_0$, resulting in a reduction of

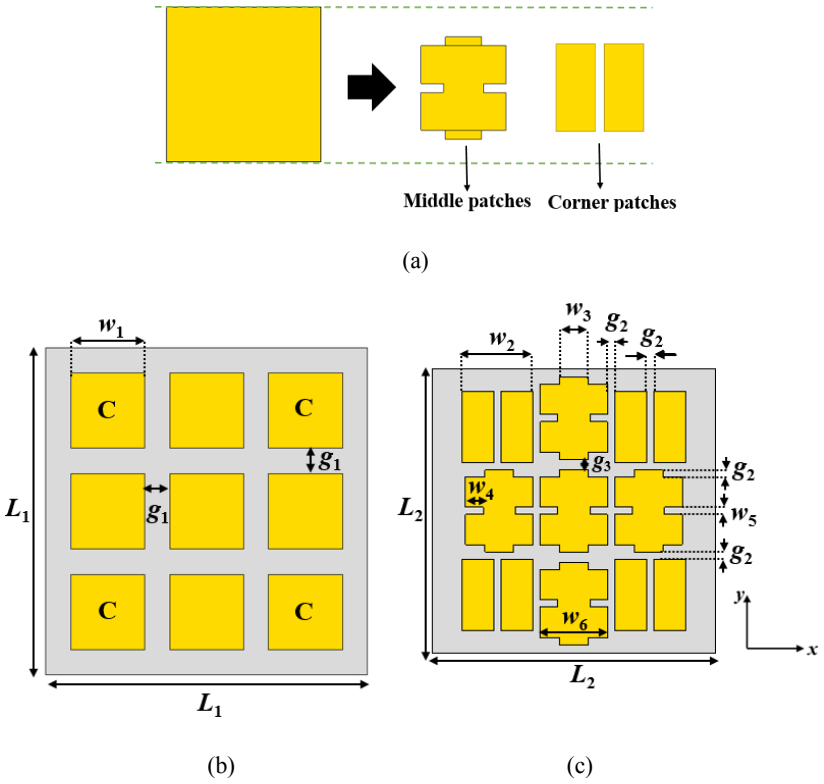

Fig. 1. (a) Unit cell evolution of the elements of the proposed metasurface, (b) uniform metasurface, (c) proposed non-uniform metasurface

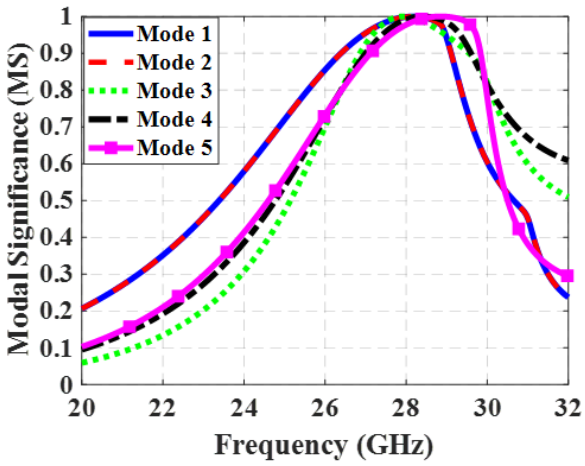

Fig. 2. MS curves of the uniform conventional metasurface

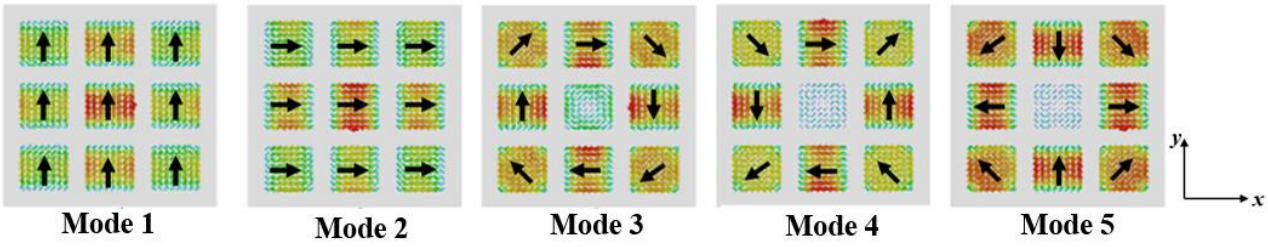

(a)

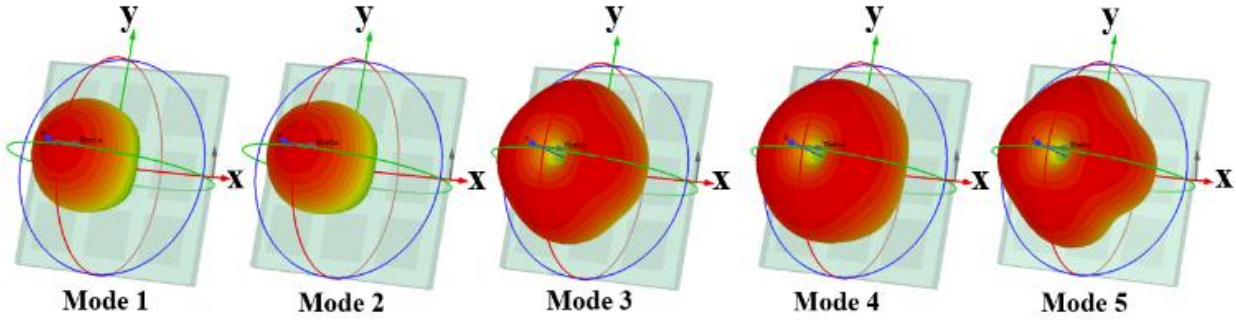

(b)

Fig. 3. (a) Modal currents and (b) far field directivity patterns of the first five characteristic modes of the uniform metasurface at 27 GHz

Table 1. Dimensions of the uniform and proposed metasurfaces

Parameter	Value (mm)	Parameter	Value (mm)
w_1	3	g_1	1
w_2	2	g_2	0.2
w_3	0.7	g_3	0.3
w_4	0.5	g_4	0.4
w_5	0.2	L_1	13
w_6	1.9	L_2	8

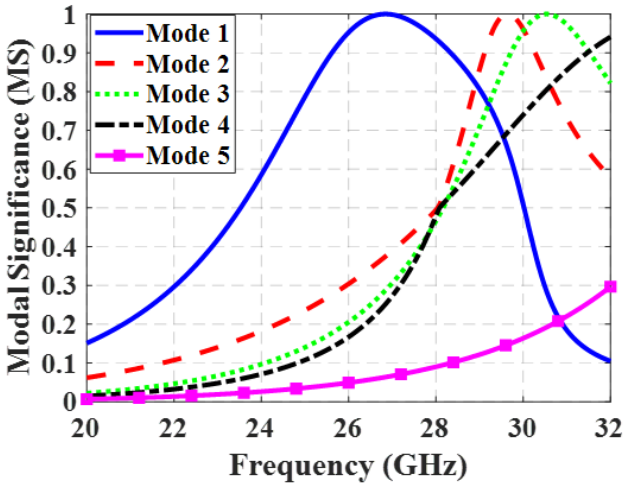

Fig. 4. MS curves of the proposed metasurface

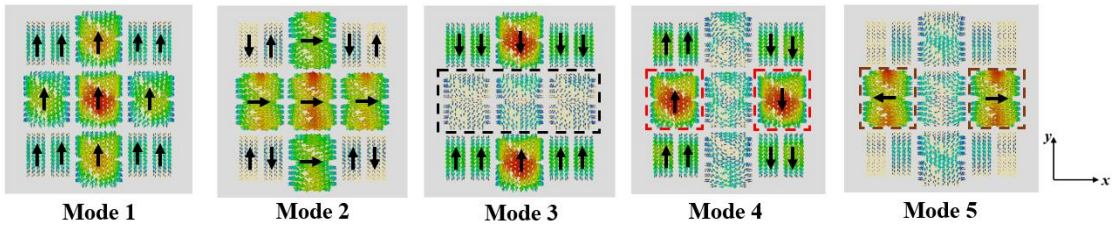

(a)

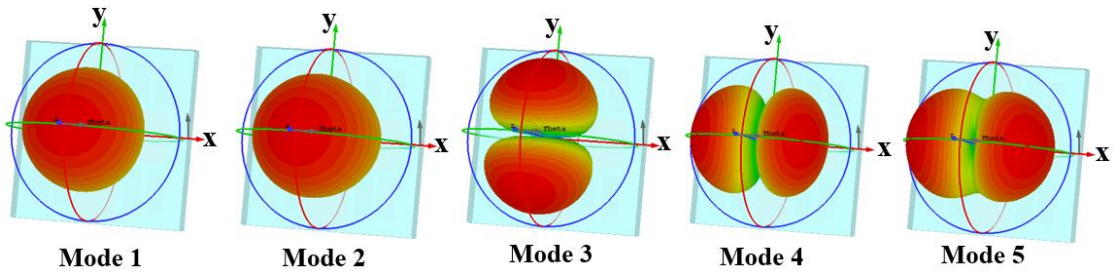

(b)

Fig. 5. (a) Modal currents and (b) far-field directivity patterns of the first five characteristic modes of the proposed metasurface at 27 GHz

approximately 62% in the occupied area, where λ_0 is free space wavelength at 27 GHz. Fig. 4 shows the MS curves of the first five characteristic modes of the proposed metasurface. It can be observed that the first and second modes are now separated, and higher-order modes have been shifted to frequencies above 28.61 GHz.

Fig. 5 illustrates the modal currents and far-field directivity patterns of the proposed metasurface. It can be observed that the first mode exhibits broadside radiation, while the surface currents of the second mode in the middle patches are perpendicular to those of the first mode. This indicates that the second mode is orthogonal to the first mode and cannot be simultaneously excited. Furthermore, the surface currents of mode 2 in the corner patches flow in opposite directions and have low magnitudes, resulting in minimal impact on the performance of the first mode. For mode 3, the weak surface currents within the central patches, as shown by the black line in Fig. 5(a), have minimal impact on the fundamental mode (mode 1). Similarly, the out-of-phase surface currents of mode 4, indicated by red lines in Fig. 5(a), require two coupling slots with differential phase feeding currents to be excited. Furthermore, the weak surface currents of mode 5

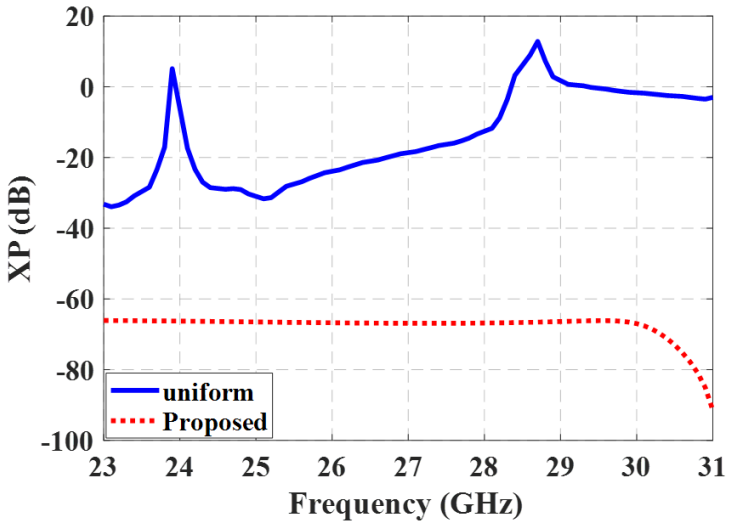

Fig. 6. XP level of the first mode for uniform and proposed metasurfaces vs. frequency at broadside direction

in most patches, or the orthogonal orientation of its currents to mode 1 in the patches indicated by brown lines, prevent it from being excited with mode 1. As a result, these higher-order modes have negligible influence on the performance of mode 1.

Fig. 6 compares the simulated XP level of the first mode for both the uniform and proposed metasurfaces vs. frequency in the broadside direction. The uniform metasurface exhibits a higher XP level and even reaches +13 dB at 28.6 GHz, whereas the proposed metasurface achieves an XP level better than -66 dB within the desired frequency range of 23.3 GHz to 30 GHz. The improved XP level in the proposed metasurface is a result of the suppression of higher-order modes, as previously discussed.

3- The proposed metasurface antenna design

The configuration of the antenna utilizing the proposed metasurface and aperture-coupled feed is depicted in Fig. 7. The first layer is made of RO4003C with ε_r = 3.55, tanδ = 0.0027, and thickness of 0.203 mm, and the second later is RT/duroid 5880 with ε_r = 2.2, and tanδ = 0.0009 and thickness of 0.787 mm. The first layer is extended to accommodate the RF connector, as shown in Fig. 7(b). The antenna is then fabricated and measured, and the fabricated prototype is shown in Fig. 8.

The reflection coefficients of the antenna, both simulated and measured, are presented in Fig. 9(a). The measured results demonstrate that the antenna effectively covers the desired 5G mm-wave band (23.3 GHz - 30 GHz) with |S11| < -10 dB. The variation of peak gain at the broadside direction across the frequency range is illustrated in Fig. 9(b), with a measured maximum gain of 8.1 dB at 28 GHz. However, there is a discrepancy between the simulated and measured results, which can be attributed to limitations in the manufacturing facilities, glue effects between the layers, and the RF connector.

The normalized radiation patterns of the antenna at two frequencies in $\varphi = 0°$ and $\varphi = 90°$ planes are presented in Fig. 10(a) and 10(b), respectively. From Fig. 10, it can be observed that in the $\varphi = 90°$ plane, the maximum XP level is -53 dB. Similarly, in the $\varphi = 0°$ plane, the maximum XP level is -26 dB. The asymmetrical feature of the antenna contributes to an increase in the XP level in the $\varphi = 0°$ plane.

The performance comparison of the proposed metasurface antenna with previously published designs is presented in Table 2. It can be observed that the present antenna has a compact size and a significantly lower XP level.

4- 2×2 MIMO antenna configuration

In the context of 5G applications, the utilization of MIMO configurations has become essential to enhance system capacity, overcome signal multipath fading, and facilitate simultaneous connections for multiple users. Consequently, the integration of smaller antennas has gained significance in these systems [10]. Nevertheless, due to the compact design of these systems, the antennas are positioned in close proximity to one another. This reduction in spacing between antenna elements leads to an increase in mutual coupling between the antennas, thereby adversely affecting the overall performance of the antenna in a multi-port system.

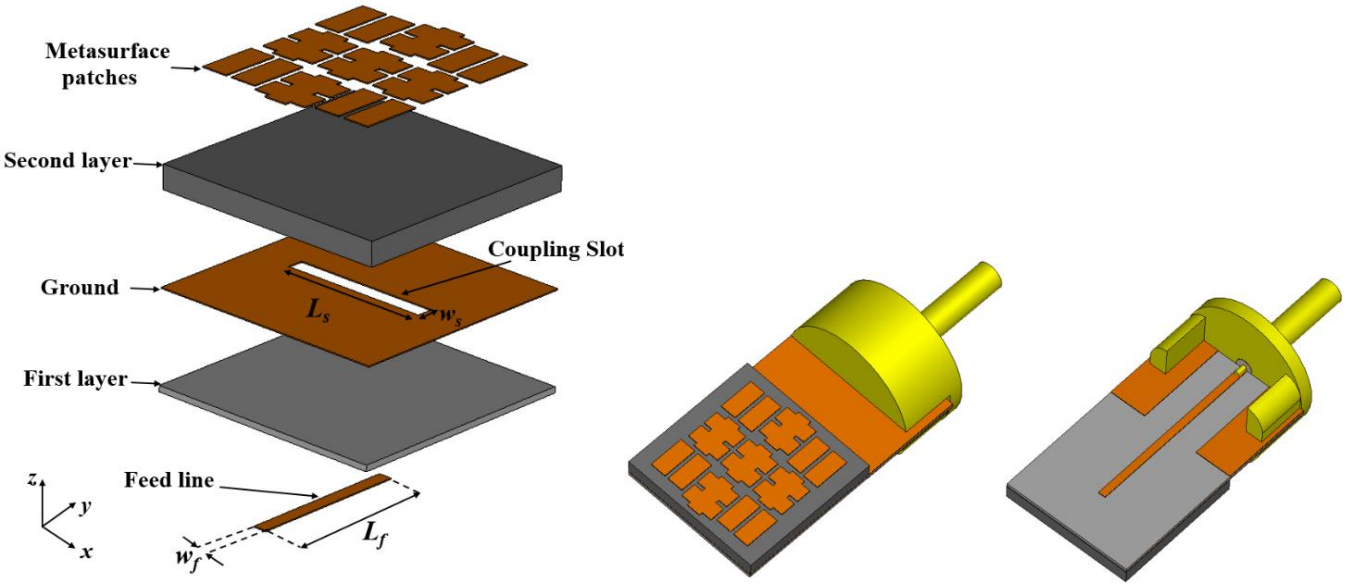

(a) (b)

Fig. 7. The configuration of the proposed metasurface antenna. (a) 3D layout of the metasurface antenna, (b) top and bottom views of the simulated antenna with a coaxial RF connector. (wf = 0.42 mm, Lf = 4.1 mm, ws = 0.55 mm, Ls = 5 mm).

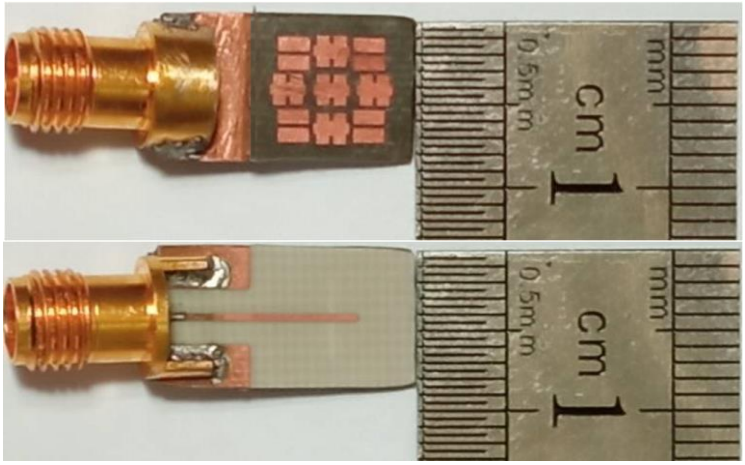

Fig. 8. Fabricated prototype of the proposed metasurface antenna

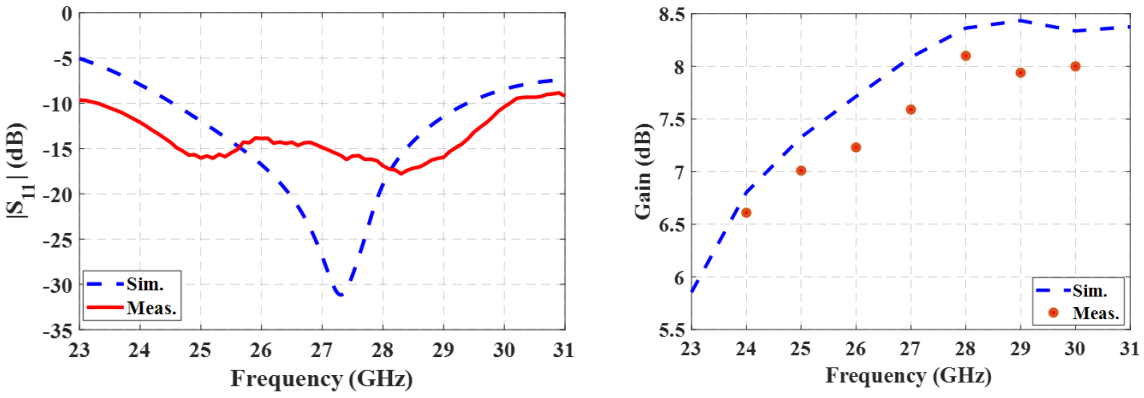

(a) (b)

Fig. 9. Simulated and measured results. (a) reflection coefficient of the proposed metasurface antenna, (b) variation of the peak gain at broadside direction vs. frequency.

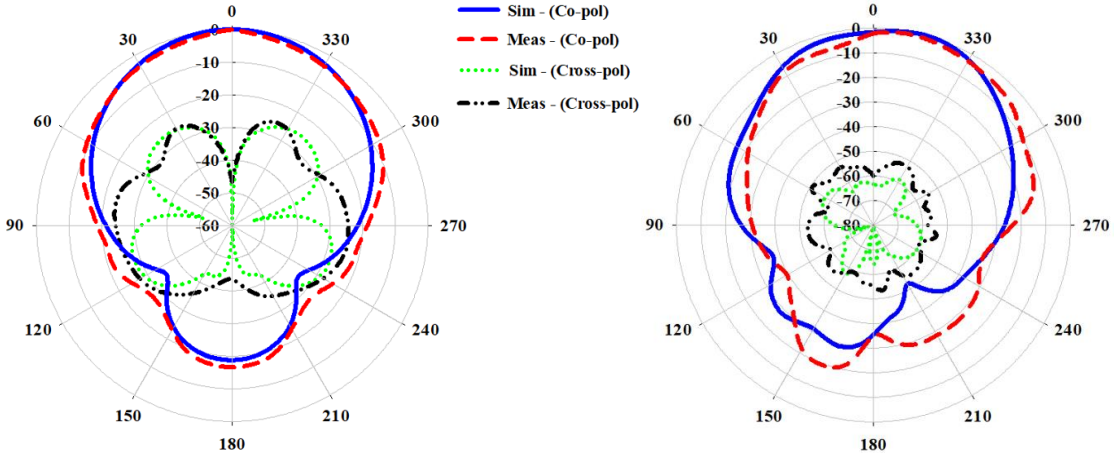

(a)

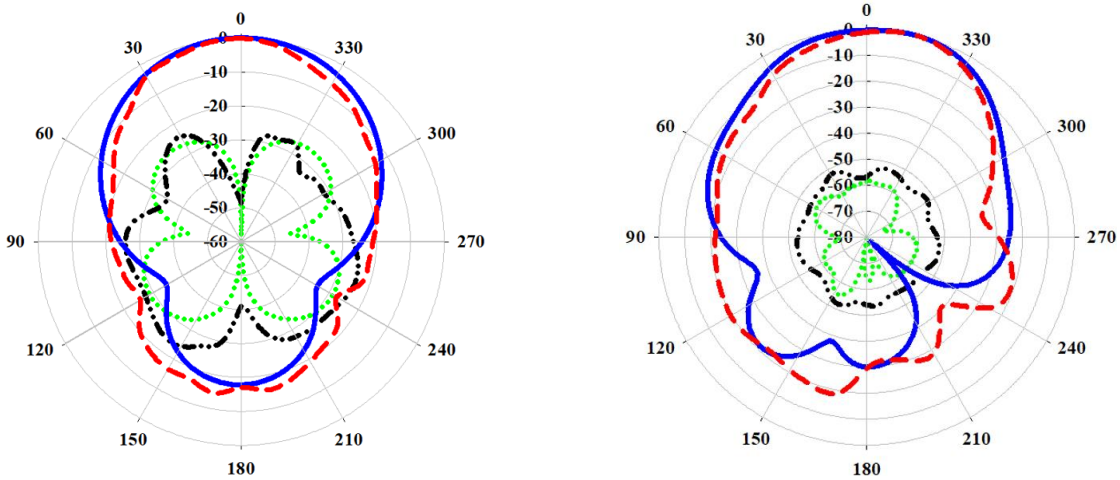

(b)

Fig. 10. Simulated and measured normaized co-pol. and cross-pol. radiation patterns of the proposed antenna in the (left) and (right) planes at two different frequencies. (a) 26 GHz, (b) 28 GHz.

Table 2. A comparison between the proposed antenna and similar metasurface antennas

Ref	Dimensions (λ_0^3)	Center Frequency (GHz)	Max. Gain (dB)	Bandwidth (%)	Efficiency (%)	XP level (dB)
[4]	1.13×1.13×0.09	5	11.6	44	Not reported	E-plane: < -19 H-plane: < -20
[7]	2.26×1.41×0.11	5.8	11.5	6.1	≥ 96	< -10
[8]	1.03×1.03×0.023	28	10.1	16	Not reported	≤ -16
[9]	1.07×1.07×0.08	6.8	9.5	32	Not reported	< -25*
This work	0.72×0.72×0.08	27	8.1	25.14	≥ 87	$\varphi = 90°$ plane: ≤ -53 $\varphi = 0°$ plane: ≤ -26

* Simulation results

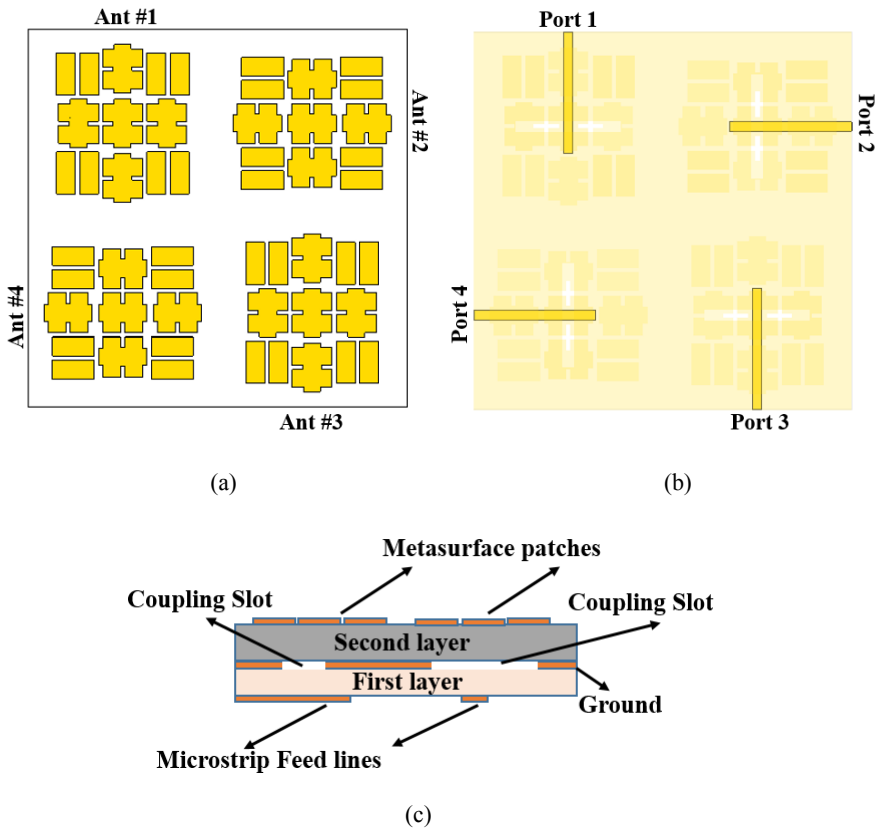

Fig. 11. Configuration of the 2×2 MIMO antenna. (a) top view, (b) bottom view, (c) side view.

In order to evaluate the performance of the proposed metasurface antenna in multi-port systems, a 2×2 MIMO configuration has been developed, as shown in Fig. 11. The antennas are positioned in close proximity to each other, without any additional spacing. The simulated S-parameters of the structure when port 1 is excited and the other ports are terminated are shown in Fig. 12.

Similar performance is observed when the other ports are excited individually due to the symmetric nature of the structure. The results demonstrate a minimum isolation of

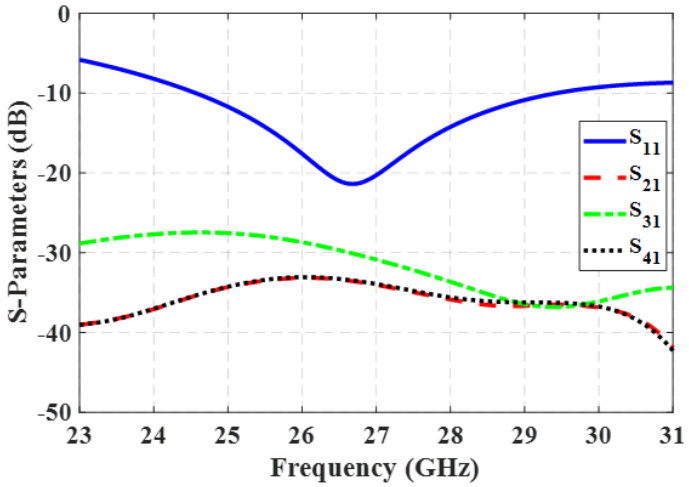

Fig. 12. Simulated S-parameters of the 2×2 MIMO antenna when port 1 is excited.

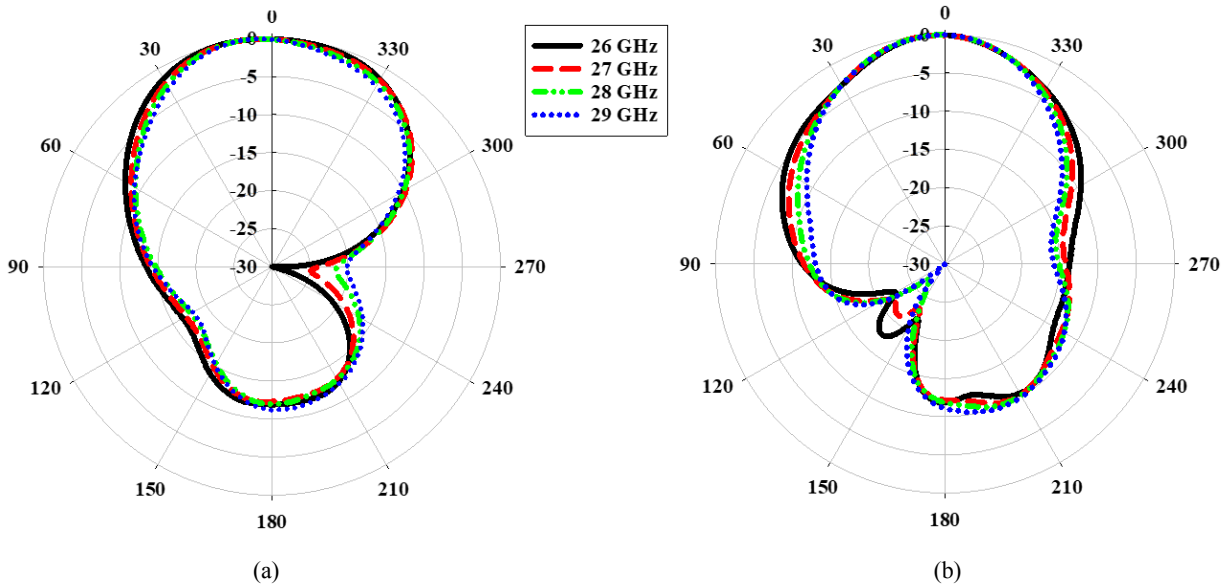

(a) (b)

Fig. 13. Normalized radiation patterns of the proposed metasurface antenna in the 2×2 MIMO configuration at different frequencies. (a) $\varphi = 0°$ plane, (b) $\varphi = 90°$ plane

27.5 dB between the elements across the entire operating frequency band. The normalized radiation patterns of the proposed antenna are depicted in Fig. 13. These patterns exhibit smooth and stable radiation, without beam squint within the desired operating frequency range. The results indicate that the performance of the proposed antenna in the MIMO configuration is not negatively affected by adjacent elements and remains consistent with that of an isolated single-element antenna.

In addition, the Envelope Correlation Coefficient (ECC) plays a vital role in evaluating the performance of MIMO systems. It measures the similarity in performance among the antennas and provides insight into their diversity. An ECC value below 0.5 is considered acceptable [12]. The ECC value is determined by Eq. (6) [12], which takes into account the 3D radiation patterns of the antennas.

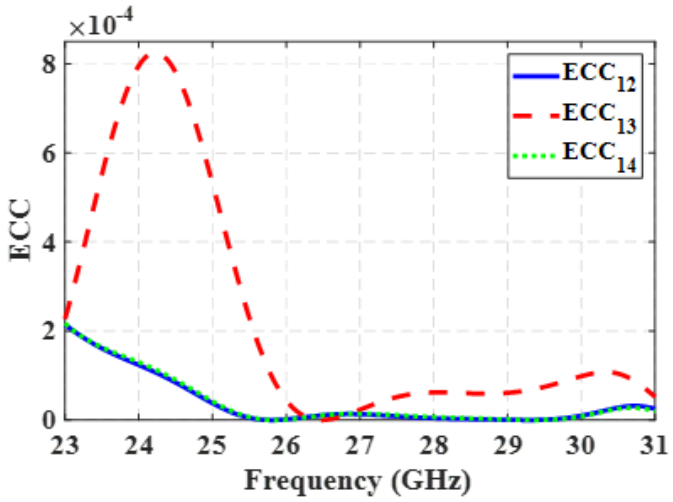

Fig. 13. ECC of the 2×2 MIMO antenna

Table 3. Comparison of the performance of the proposed antenna with other antennas in a 2×2 MIMO configuration

Antenna	Beam Split	Center Frequency (GHz)	Bandwidth (%)	Beam squint angle (°)	Complexity
[3]	No	5.5	24	(2) ~ (8)	High with air gap layer and pins
[14]	No	5.8	3.44	*xy* plane: (-8) ~ (-4) *zy* plane: (17) ~ (28)	Medium with modifications in the ground plane
[15]	Yes	26	22.69	(-30) ~ (30)	Medium with air gap layer
This work	No	27	25.14	$\varphi = 90°$ plane: (-2) ~ (2) $\varphi = 0°$ plane: 0	Simple

$$\mathrm{ECC}_{mn} = \frac{\left| \int_0^{4\pi} \int [\vec{F}_m(\theta,\phi) \times \vec{F}_n(\theta,\phi)] d\Omega \right|^2}{\int_0^{4\pi} \int \left|\vec{F}_m(\theta,\phi)\right|^2 d\Omega \int_0^{4\pi} \int \left|\vec{F}_n(\theta,\phi)\right|^2 d\Omega} \quad (6)$$

where m and n are the numbers of the antennas, $\vec{F}_m(\theta,\phi)$ and $\vec{F}_n(\theta,\phi)$ represent the 3D radiation patterns of the Ant #m and Ant #n, respectively, and $d\Omega$ denote the solid angle. The ECC values for the 2×2 MIMO configuration of the proposed metasurface antenna are shown in Fig. 14. It can be observed that the ECC value consistently stays below 0.00082 throughout the frequency range, indicating the satisfactory diversity performance of the proposed antenna.

Table 3 provides a comparison of the performance of the proposed antenna with other antennas in a 2×2 MIMO configuration. The use of the proposed metasurface antenna results in reduced beam squint angles in the radiation patterns. Moreover, our design eliminates the requirement for multiple short pins, as opposed to the antenna structure proposed in [3], thereby simplifying the overall fabrication process of the antenna.

5- Conclusion

This paper introduces a metasurface antenna that is well-suited for 5G mm-wave applications due to its low profile, compact size, and low cross-polarization level. By strategically incorporating slits and stubs in the middle patches, as well as rectangular slots in the corner patches of the proposed metasurface, the first two degenerate modes are effectively separated, and unwanted higher-order modes are pushed to frequencies above 28.61 GHz. Compared to a uniform metasurface, the overall dimensions of the antenna are reduced by 62%, while maintaining a measured cross-polarization level below -26 dB and -53 dB at $\varphi = 0°$ and $\varphi = 90°$ planes, respectively, across the entire frequency band (23.3 GHz - 30 GHz). Additionally, the performance of the proposed metasurface antenna was evaluated in a 2×2 MIMO configuration. The displacement of unwanted higher-order modes to higher frequencies resulted in significant improvements in issues such as radiation pattern ripples, beam splitting, and beam squint commonly observed in uniform metasurface antennas. Overall, this antenna is highly suitable for use in 5G mm-wave MIMO systems.

Acknowledgment

The authors would like to express their gratitude to the MCI R&D Center for their valuable financial support in carrying out this research.

References

[1] M.A. Jensen, J.W. Wallace, A review of antennas and propagation for MIMO wireless communications, IEEE Transactions on Antennas and propagation, 52(11) (2004) 2810-2824.

[2] I. Nadeem, D.-Y. Choi, Study on mutual coupling reduction technique for MIMO antennas, IEEE Access, 7 (2018) 563-586.

[3] F.H. Lin, Z.N. Chen, A method of suppressing higher order modes for improving radiation performance of metasurface multiport antennas using characteristic mode analysis, IEEE Transactions on antennas and propagation, 66(4) (2018) 1894-1902.

[4] Z.Z. Yang, F. Liang, Y. Yi, D. Zhao, B.Z. Wang, Metasurface-based wideband, low-profile, and high-gain antenna, IET Microwaves, Antennas & Propagation, 13(4) (2019) 436-441.

[5] W. Liu, Z.N. Chen, X. Qing, Metamaterial-based low-profile broadband mushroom antenna, IEEE Transactions on antennas and propagation, 62(3) (2013) 1165-1172.

[6] S. Pandi, C.A. Balanis, C.R. Birtcher, Design of scalar impedance holographic metasurfaces for antenna beam formation with desired polarization, IEEE transactions on antennas and propagation, 63(7) (2015) 3016-3024.

[7] K. Wang, W. Shao, X. Ding, B.-Z. Wang, B. Jiang, Design of high-gain metasurface antenna based on characteristic mode analysis, IEEE Antennas and Wireless Propagation Letters, 21(4) (2022) 661-665.

[8] M. Xue, W. Wan, Q. Wang, L. Cao, Low-profile millimeter-wave broadband metasurface antenna with four resonances, IEEE Antennas and Wireless Propagation Letters, 20(4) (2021) 463-467.

[9] J. Xue, W. Su, Z. Li, B. Wu, Broadband Metasurface Antenna with Low Cross-polarization Based on Characteristic Theory, in: 2021 IEEE MTT-S International Wireless Symposium (IWS), IEEE, 2021, pp. 1-3.

[10] S. Li, Z.N. Chen, T. Li, F.H. Lin, X. Yin, Characterization of metasurface lens antenna for sub-6 GHz dual-polarization full-dimension massive MIMO and multibeam systems, IEEE Transactions on Antennas and Propagation, 68(3) (2020) 1366-1377.

[11] Y. Chen, C.-F. Wang, Characteristic modes: Theory and applications in antenna engineering, John Wiley & Sons, 2015.

[12] M. Ikram, E. Al Abbas, N. Nguyen-Trong, K.H. Sayidmarie, A. Abbosh, Integrated frequency-reconfigurable slot antenna and connected slot antenna array for 4G and 5G mobile handsets, IEEE Transactions on Antennas and Propagation, 67(12) (2019) 7225-7233.

[13] R. Zaker, Design of a very closely-spaced antenna array with a high reduction of mutual coupling using novel parasitic L-shaped strips, International Journal of RF and Microwave Computer-Aided Engineering, 28(9) (2018) e21422.

[14] E. Fritz-Andrade, A. Perez-Miguel, R. Gomez-Villanueva, H. Jardon-Aguilar, Characteristic mode analysis applied to reduce the mutual coupling of a four-element patch MIMO antenna using a defected ground structure, IET Microwaves, Antennas & Propagation, 14(2) (2020) 215-226.

[15] D.A. Sehrai, M. Asif, W.A. Shah, J. Khan, I. Ullah, M. Ibrar, S. Jan, M. Alibakhshikenari, F. Falcone, E. Limiti, Metasurface-based wideband MIMO antenna for 5G millimeter-wave systems, IEEE Access, 9 (2021) 125348-125357.

HOW TO CITE THIS ARTICLE

H. Hamlbar-Gerami, R. Kazemi, A Low-Profile Metasurface MIMO Antenna with Suppressed Higher-Order Modes for 5G Applications. AUT J Electr Eng, 56(2) (2024) 153-164.

DOI: 10.22060/eej.2023.22533.5548